Journal of Hazardous Materials 192 (2011) 1409–1417

Contents lists available at ScienceDirect

Journal of Hazardous Materials

journal homepage: www.elsevier.com/locate/jhazmat

Sorption of polycyclic aromatic hydrocarbons on electrospun nanofibrous membranes: Sorption kinetics and mechanism

Yunrong Dai, Junfeng Niu*, Lifeng Yin, Jiangjie Xu, Yaohong Xi

State Key Laboratory of Water Environment Simulation, School of Environment, Beijing Normal University, Beijing 100875, PR China

ARTICLE INFO

Article history:
Received 13 April 2011
Received in revised form 18 June 2011
Accepted 20 June 2011
Available online 24 June 2011

Keywords:
Electrospun nanofibrous membranes
PAHs
Water treatment
Sorption isotherm
Sorption mechanisms

ABSTRACT

Five types of nanofibrous membranes were prepared by electrospinning poly(ε-caprolactone) (PCL), poly(D,L-lactide) (PDLLA), poly(lactide-co-caprolactone) (P(LA/CL)), poly(D,L-lactide-co-glycolide) (PDLGA) and methoxy polyethylene glycol-poly(lactide-co-glycolide) (MPEG-PLGA), respectively. These electrospun nanofibrous membranes (ENFMs) were used to adsorb anthracene (ANT), benz[*a*]anthracene (BaA) and benzo[*a*]pyrene (BaP) from aqueous solution, and the sorption kinetics and isotherms of these PAHs on the five ENFMs were investigated. The pseudo-second-order model (PSOM) can well describe the sorption kinetics of the three PAHs on five ENFMs, and the partition-adsorption model (PAM) can interpret the sorption processes of PAHs on the ENFMs. PCL ENFMs, which had the largest surface areas ($8.57\ m^2\ g^{-1}$), exhibited excellent sorption capacity for ANT at over $4112.3 \pm 35.5\ \mu g\ g^{-1}$. Moreover, the hydrophobicity and pore volume of ENFMs significantly affected the sorption kinetics and sorption capacity of the PAHs. The main sorption mechanisms of three PAHs on the PDLLA ENFMs included hydrophobic interactions and pore-filling, while those of PCL, P(LA/CL) and PDLGA ENFMs were dominated by the hydrophobic interactions. The sorption mechanisms of MPEG-PLGA ENFMs primarily included pore-filling, hydrogen bonding interactions and hydrophobic interactions. Additionally, π–π bonding interaction was also deduced to be involved in all of ENFMs sorption systems.

1. Introduction

Polycyclic aromatic hydrocarbons (PAHs) are persistent toxic pollutants consisting of two or more fused benzene rings. As products of the incomplete combustion of hydrocarbons and other organic matters, such as coal, petroleum and biomass, PAHs eventually enter into the aquatic environment via atmospheric deposition, industrial and/or municipal effluent discharges, and agricultural runoffs [1,2]. Due to their stable poly-condensed aromatic structure, PAHs can be transported over long distances in water and be widely distributed in aquatic ecosystems. Some PAHs with four or more benzene rings, such as benzo[*a*]anthracene, chrysene and benzo[*a*]pyrene, have been shown to be carcinogenic, representing a considerable ecosystems and human health hazard [3–6]. Many rivers and lakes around the world were reported to have been polluted by PAHs to different degrees, and the concentrations of PAHs in waters have reached the level of several micrograms per liter [7–9]. Therefore, an urgent attention to the effective treatment of PAHs is desired.

Several methods have been proposed for the removal of PAHs from the aquatic environment, including ozone oxidation [10], photocatalysis [11–13], biodegradation [14], sorption [15,16], and so on. Among these methods, sorption treatment is widely applied because it provides a simple and cost-effective approach for the removal of PAHs. Various types of sorbents, including activated carbons [17], resins [18], carbon nanomaterials [19] and bentonite [16], have been reported to be effective for PAH removal. However, these sorbents, which generally exist in the form of powders or particles, are difficult to be recycled from water, thus restricting their practical application in water treatment.

Electrospun nanofibrous membranes (ENFMs) are composed of non-woven nanofibers fabricated by electrospinning, which is a simple and low-cost technique [20–22]. Since ENFMs possess many extraordinary properties including high surface-to-volume ratios, porous structures, and resultant superior mechanical properties, they have attracted considerable attentions and have been extensively used in tissue engineering, biomedicine, as well as enzyme immobilization [23–25]. In recent years, applications of ENFMs in environmental remediation and sample pretreatment have sparked increasing interests [26]. For example, ENFMs have been successfully developed into high-performance air filters, showing extremely effective removal (~100% rejection) of airborne particles with diameters between 1 and 5 μm [27]. Moreover, different poly-

* Corresponding author. Tel.: +86 10 5880 7612; fax: +86 10 5880 7612.
E-mail address: junfengn@bnu.edu.cn (J. Niu).

0304-3894/$ – see front matter © 2011 Elsevier B.V. All rights reserved.
doi:10.1016/j.jhazmat.2011.06.055

mers may be electrospun into membranes, and these ENFMs have been used for the effective removal of heavy metal ions and various organic compounds in waters [26], such as phenolphthalein, humic acid and oil. Some research groups have explored the feasibility of using poly(styrene-co-methacrylic acid), poly(styrene-co-*p*-styrene sulfonate), polystyrene and nylon6 (–[NH-$(CH_2)_5$-CO]$_n$–) ENFMs as solid-phase extraction (SPE) sorbents to directly extract trace organic pollutants from environmental water [28,29]. Their results indicated that the ENFMs possessed excellent sorption properties and exhibited significant potential for the enrichment of organic pollutants in the water samples. Furthermore, compared with other powdered or granular sorbents, the membrane sorbents can be used directly and easily separated from the reaction solution after sorption. Therefore, ENFMs are viewed as a kind of potential sorbent. However, few researches about the sorption of PAHs from aqueous solution using ENFMs have been reported, and the sorption behaviors and mechanisms of PAHs on ENFMs have not been fully elucidated and understood.

The aim of the present study was to prepare the nanofibrous membranes by electrospinning five types of polymers with different structures and properties, including poly(ε-caprolactone) (PCL), poly(D,L-lactide) (PDLLA), poly(lactide-co-caprolactone) (P(LA/CL)), poly(D,L-lactide-co-glycolide) (PDLGA) and methoxy polyethylene glycol-poly(lactide-co-glycolide) (MPEG-PLGA). These polymers were selected because they have good mechanical properties and spinnability. In addition, all of them are completely biodegradable polymers, and will not cause secondary pollution. The five ENFMs were used to adsorb the probable human carcinogenic PAHs from aqueous solution. The sorption kinetics and isotherms of anthracene (ANT), benz[*a*]anthracene (BaA) and benzo[*a*]pyrene (BaP) on the five ENFMs were investigated. The sorption mechanisms and the possible interactions between the sorbents and sorbates were also discussed.

2. Materials and methods

2.1. Materials

Poly(ε-caprolactone), poly(D,L-lactide), poly(lactide-co-caprolactone), poly(D,L-lactide-co-glycolide) and methoxy polyethylene glycol-poly(lactide-co-glycolide) were provided by Jinan Daigang biomaterials Co., Ltd. (Shandong, China). The molecular weight of each polymer was approximately 100 000, and their structural formulas are shown in Fig. 1. Methylene dichloride and methanol (HPLC, 99.9%) were purchased from JTBaker (USA). Anthracene (ANT, 99.5%), benz[*a*]anthracene (BaA, 99.7%) and benzo[*a*]pyrene (BaP, 99.0%) were obtained commercially from Sigma–Aldrich (USA), and some of their properties are summarized in Table S1 (see Supporting Information). All other reagents and solvents were analytical grade and used without further purification. All solutions were prepared using high-purity water obtained from a Milli-Q Plus/Millipore purification system (USA).

2.2. Preparation of electrospun nanofibrous membranes

Electrospinning was carried out on a self-made electrospinning apparatus in our laboratory. The procedure for the electrospun nanofibrous membranes (ENFMs) was as follows: firstly, an appropriate amount of polymer was dissolved in methylene dichloride with gentle stirring for 3 h at ambient temperature to form a homogeneous solution. The polymer concentrations of PCL, PDLLA, P(LA/CL), PDLGA and MPEG-PLGA were maintained at 6, 9, 4, 7 and 8 wt% in methylene dichloride, respectively. The solution was then loaded into a glass syringe equipped with a stainless needle (0.5 mm inner diameter), which was connected with a high-voltage power supply (HB-Z503-2AC, Tianjin Hengbo High-voltage Power Supply Plant, China). Electrospinning was performed at a voltage of about

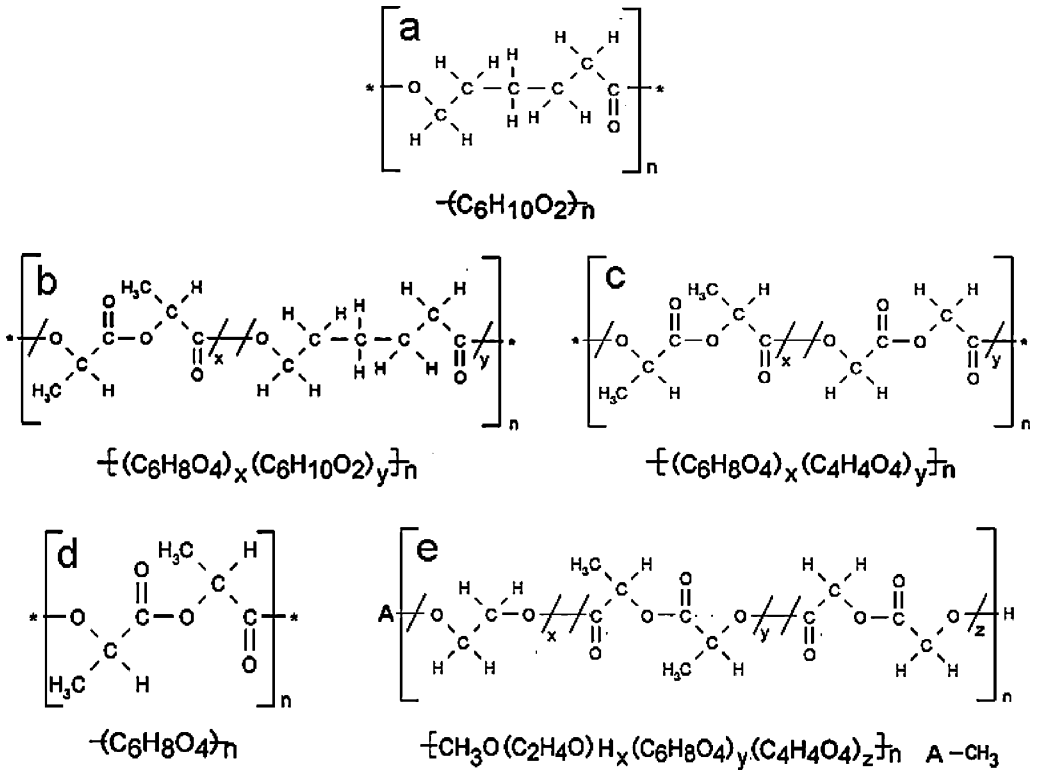

Fig. 1. Chemical structure and molecular formula of the polymers: (a) PCL; (b) P(LA/CL); (c) PDLGA; (d) PDLLA; and (e) MPEG-PLGA.

Table 1
Selected structural properties of five ENFMs.

Adsorbent (ENFMs)	Average diameter (nm)	A_{surf}[a] ($m^2\ g^{-1}$)	V_{total}[b] ($cm^3\ g^{-1}$)	Contact angle[c] (°)
PCL	200 ± 20	8.57	0.0096	72.7
P(LA/CL)	300 ± 15	6.96	0.0052	86.6
PDLLA	500 ± 20	5.23	0.0163	95.1
PDLGA	600 ± 35	3.55	0.0068	70.3
MPEG-PLGA	850 ± 30	1.98	0.0209	57.0

[a] Surface area, calculated from the adsorption–desorption isotherm of N_2 at 77 K by multi-point BET.
[b] Single point adsorption total pore volume.
[c] Contact angle of polymer.

15 kV. A syringe pump (RWD Life Science Co., Ltd, China) delivered the solution at a flow rate of 1.5 mL h^{-1} using a 10 mL syringe. A grounded iron plate covered with aluminum foil was placed at a distance of 15 cm from the needle tip as a fiber collector. It usually took 4–5 h to obtain sufficiently thick and integrated ENFMs. The ENFMs were dried in a vacuum for 10 h to remove residual solvent before use. In this study, five types of polymer/methylene dichloride solution with different concentrations were used for electrospinning. Each polymer solution concentration was selected based on the formation of stable jets and bead-free fibers during electrospinning, when the voltage, solution flow rate, distance between the needle tip and the collecting plate were kept constant. All experiments were conducted at room temperature (25 ± 1 °C) and a relative humidity of about 40 ± 2%.

2.3. Characterization

The morphology of the ENFMs was observed with a field emission scanning electron microscope (FESEM S-4800, Hitachi, Japan). The average fiber diameter was taken by randomly selecting 100 counts from 10 different SEM images for each sample. Fourier transform infrared spectroscopy (FTIR, Nexus 670, USA) was used to analyze the surface properties of different ENFMs. The specific surface area and pore volume of the ENFMs were determined using a full-automatic specific surface area analyzer (ASAP 2020, Micromeritics, USA). In order to measure the hydrophilic–hydrophobic properties of the materials, the polymers were dissolved in methylene dichloride and prepared into cast films, and the contact angles were tested on a contact angle measuring system (OCA20, Dataphysics, Germany). The properties of ENFMs are shown in Table 1.

2.4. Sorption experiments

Batch experiments were conducted at 25 ± 1 °C in an incubator shaker. Three pieces of ENFMs (1 cm × 1 cm, total weight 50–55 mg) were added to 100 mL aqueous solution of PAHs, and the reaction mixture was incubated with stirring (120 rpm). In our experiments, sorption kinetics was determined from solutions with 40 μg L^{-1} of PAHs. The sorption isotherm experiments were conducted with an initial PAH concentration ranging from 10 to 100 μg L^{-1}. The methanol volume fraction in each solution was controlled to less than 0.001 to avoid cosolvent effect. At specific time point, a volume of 0.5 mL sample was taken from reaction system for high-performance liquid chromatography (HPLC; Dionex U3000, USA) analysis. Experimental uncertainties evaluated in vials without ENFMs were less than 5% of the initial concentrations. The pH values of the reaction solutions during the sorption process were monitored, which showed they were practically unchanged. All experiments were conducted twice, and the average value was adopted.

2.5. Sorption kinetics and isotherm models

Among all the sorption kinetic models, the pseudo first order (PFOM) and pseudo second order (PSOM) models are frequently used. Some researchers advised that the modified PFOM and PSOM have higher adaptability to sorption kinetic data [30], thus the modified PFOM and PSOM was adopted in the present study. Since ENFMs are porous sorbents, the intra fiber diffusion may exist in the sorption processes, the intraparticle diffusion model proposed by Weber and Morris (WMM) was also used to describe the data. Three sorption isotherm models, the Freundlich (FM), partition-adsorption (PAM) and Polanyi theory-based Dubinin-Ashtakhov

Table 2
Models used for fitting of sorption kinetics and isotherm in this study.

Category	Name	Abbreviation	Equation	Capacity term
Sorption kinetics models	Pseudo-first order model	PFOM	$q_t = q_e(1 - e_1^{-kt})$	k_1 [h^{-1}], rate constant of the pseudo-first order model
	Pseudo-second order model	PSOM	$q_t = q_e k_2^* t/(1 + k_2^* t)$	$k_2^* = k_2 q_e$ [h^{-1}]; k_2, the rate constant of the pseudo-second order equation
	Intra particle diffusion model of Weber and Morris	WMM	$q_t = C + k_{WM} t^{1/2}$	k_{WM} [$h^{-1/2}$], intra particle diffusion rate constant of Weber and Morris
Sorption isotherm models	Freundlich model	FM	$q_e = K_f C_e^{1/n}$	K_f [$((\mu g\ g^{-1})(\mu g\ L^{-1})^{n-1})^{-1}$], Freundlich affinity coefficient; $1/n$, Freundlich exponential coefficient
	Partition-adsorption model	PAM	$q_e = K_P C_e + Q^0 C_e/(K_d + C_e)$	K_P [$L\ g^{-1}$], partition coefficient; K_d [$\mu g\ L^{-1}$], affinity coefficient
	Polanyi theory-based Dubinin-Ashtakhov model	PDAM	$\log q_e = \log Q^0 + (\varepsilon_{sw}/E)^b$	$\varepsilon_{sw} = -RT\ln(C_e/C_s)$ [kJ mol^{-1}], effective adsorption potential, where R [8.314×10^{-3} kJ $(mol\ K)^{-1}$] and T [K]; E [kJ mol^{-1}], correlating divisor; b, fitting parameter.

q_e, equilibrium sorption amount (μg g^{-1}); C_e, equilibrium solution phase concentration (μg L^{-1}); Q^0, sorption capacity (μg g^{-1}); S_w, water solubility (mg L^{-1}); q_t, sorption amount at time t (μg g^{-1}); C, intercept (μg g^{-1}).

(PDAM) equations were applied to fit the experimental data. Mean weighted square error (MWSE), expressed as $1/\nu[(q_{measured} - q_{model})/q^2_{measured}]$, and correlation coefficients (r^2) were used to evaluate the goodness of model fitting; where ν is the degree of freedom ($\nu = N-2$ for FM; $\nu = N-3$ for PAM and PDAM), N is the number of experimental data points, $q_{measured}$ is the measured equilibrium sorbed amount, and q_{model} stands for the estimated equilibrium sorbed amount by the respective models [19]. The sorption kinetics and isotherm models are listed in Table 2.

3. Results and discussion

3.1. Morphology of electrospun nanofibrous membranes

The SEM images of five ENFMs which are shown in Fig. 2, illustrate that these nanofibers possess a common feature of being bead-free and randomly arrayed. However, the sizes of five kinds of fibers were remarkably different. The average diameters of PCL and P(LA/CL) fibers were approximately 200 and 300 nm, respectively. But larger fiber diameters were obtained when electrospinning other polymer solutions, and the average diameters of the MPEG-PLGA fibers reached 850 ± 30 nm. Furthermore, different porous fibers were observed for the five types of fibers. As shown in Fig. 2d and e, the PDLLA and MPEG-PLGA fibers show numerous pores with an average size of tens of nanometers. While the pores on the surface of the three other fibers were difficult to be seen in the SEM images, and the determination of the pore volume has proved the existence of pores on the surface of the fibers. Variations in polymers and their concentration led to the changes in solution properties, such as viscosity, surface tension, and net charge density, which can significantly influence the size and morphology of the fibers [20,21]. The distinctions in pore morphologies of these electrospun fibers may mainly attributed to the different properties

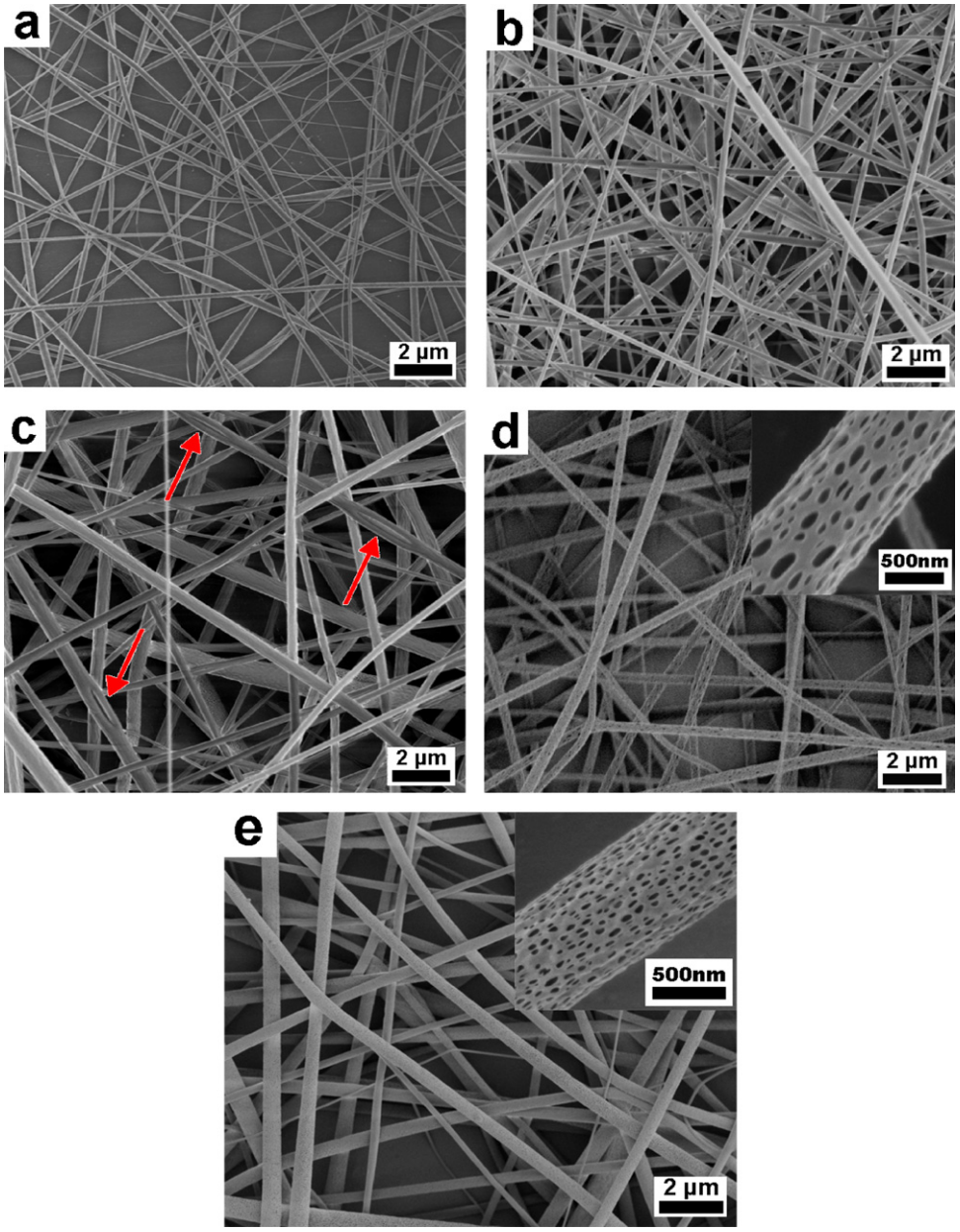

Fig. 2. SEM micrographs of ENFMs: (a) PCL ENFMs; (b) P(LA/CL) ENFMs; (c) PDLGA ENFMs; (d) PDLLA ENFMs; and (e) MPEG-PLGA ENFMs. The red arrowheads in image (c) show the grooved areas on the surface of PDLGA fibers; and the inserted images in (d) and (e) show the enlarged image of the pores on the surface of fibers. (For interpretation of the references to color in this figure legend, the reader is referred to the web version of this article.)

of five polymer/solvent systems, which influence the phase separation in the electrospinning. Since phase separation in polymer-rich and polymer-poor regions occurs during the evaporation of the solvent, and the pores are more likely to form in the polymer-poor region of fibers [20]. Moreover, the electrospinning parameters may also affect the formation and morphology of pores [22]. The porous structures on fibrous surface are recognized as being advantageous because they can increase the surface area and offer some spaces and sites for sorbing the adsorbates.

3.2. Sorption kinetics

Fig. 3 shows the sorption kinetics of ANT, BaA and BaP on five ENFMs. All the sorption processes were mostly achieved within the first 30 min of reaction, and then became more gradual until the equilibrium was reached after 3 h. Although the sorption trends of the PAHs on the ENFMs adsorbents were similar, their kinetic profiles were obviously different. The sorption rates of the PCL ENFMs for PAHs were relatively faster than others, and its sorption capacity for ANT, BaA and BaP reached 75.6, 78.3 and 73.5 $\mu g\,g^{-1}$ at 60 min, respectively. This may be mainly attributed to the highest surface area of PCL ENFMs. However, the amount of ANT, BaA and BaP adsorbed on the MPEG-PLGA ENFMs was only 56.3, 55.1 and 53.7 $\mu g\,g^{-1}$ at 60 min, respectively. The smallest surface area, the highest hydrophilic property and the porous structure may result in the relatively slow sorption rates of the MPEG-PLGA ENFMs for PAHs.

To understand the sorption kinetics further, the modified PFOM and PSOM were applied to describe the sorption kinetics data. The estimated correlation coefficient (r^2) demonstrated that the PSOM fitted the experimental data better than the PFOM, as shown in Table S2. The modified parameter of k_2^* was considered to be a more applicable rate constant to directly describe adsorption kinetic process based on PSOM [30]. The rate constants (k_2^*) of the three PAHs on most ENFMs, including PCL, P(LA/CL) and MPEG-PLGA ENFMs, were ranked in the order of ANT > BaA > BaP (shown in Table S2), which was inversely related to the variation of $\log K_{ow}$ (shown in Table S1). However, the rate constants (k_2^*) of the three PAHs on the most hydrophobic PDLLA ENFMs showed a positive relationship with $\log K_{ow}$. For a given adsorbate, the k_2^* value is mainly determined by the surface area of the ENFMs, showing positive correlation; meanwhile, it is related to the hydrophilic–hydrophobic properties of the polymers. Moreover, it was also found that the initial sorption rate (υ_0) of the PDLGA ENFMs was faster than that of the other ENFMs. This phenomenon may be mainly attributed to the defected areas of PDLGA fibers (shown in Fig. 2c), which were regarded as the high-energy adsorption sites and resulted in high sorption rate at lower concentration [31].

The WMM was adopted to fit the sorption kinetics since the PSOM cannot provide a definite process for sorption, Weber and Morris illustrated that if intra sorbent diffusion is the sole rate-controlling factor in a system, a good linear relationship should be obtained from the plot of adsorbate uptake (q_t) vs. the square root of time ($t^{1/2}$), and the line should also pass through the origin [32–33]. As shown in Fig. 4 and Table S2, the WMM fitted the sorption data of ANT on the five ENFMs well, according to the relatively high correlation coefficients obtained ($r^2 > 0.93$), but the plots did not pass through the origin. This implies that intra sorbent diffusion may be a rate-controlling step for ANT sorption on the ENFMs, but it is not the only one. The sorption rate may also be influenced by the morphology and nature properties of the adsorbent, the concentration of adsorbate, and its affinity to the adsorbent [34]. It was also discovered that the plots obtained from the data of BaA and BaP on PCL, P(LA/CL) and PDLGA ENFMs not only had significant positive intercepts but also displayed poor linearity (shown in Fig. 4b and c). Since the molecule sizes of BaA and BaP are larger than that of ANT, and the pores volumes of PCL, P(LA/CL) and PDLGA ENFMs are relatively smaller, the intra sorbent diffusions of BaA and BaP are inconspicuous, and thus they are not the rate-controlling factors. However, the intra sorbent diffusion is a possible rate-controlling

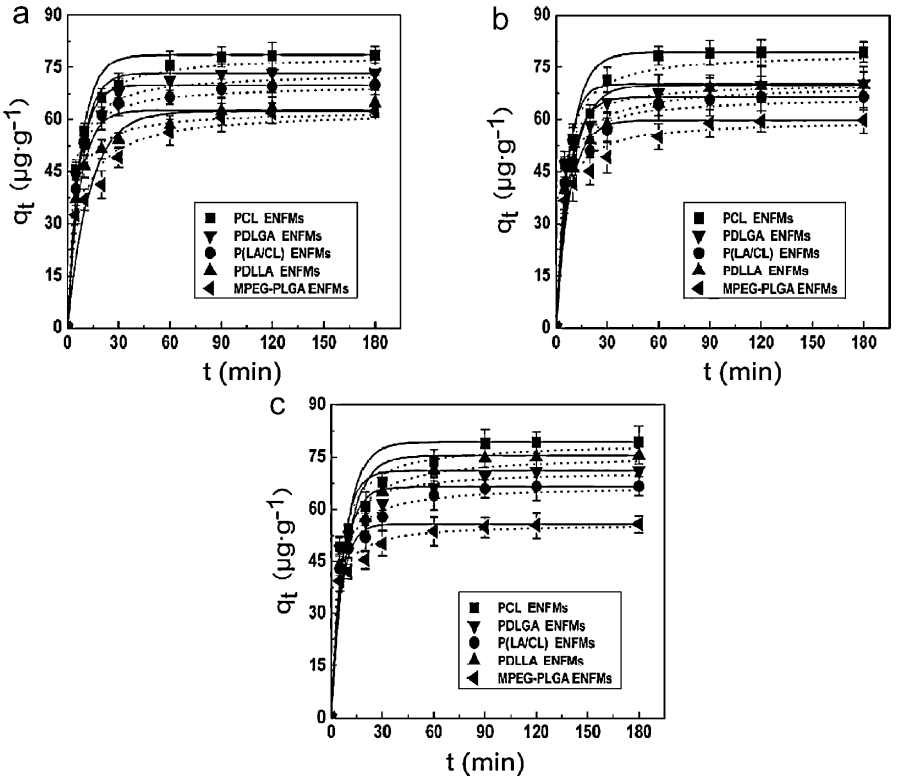

Fig. 3. Sorption kinetics of ANT (a), BaA (b) and BaP (c) on five ENFMs fitted by the pseudo-first-order model (––) and pseudo-second-order model (...).

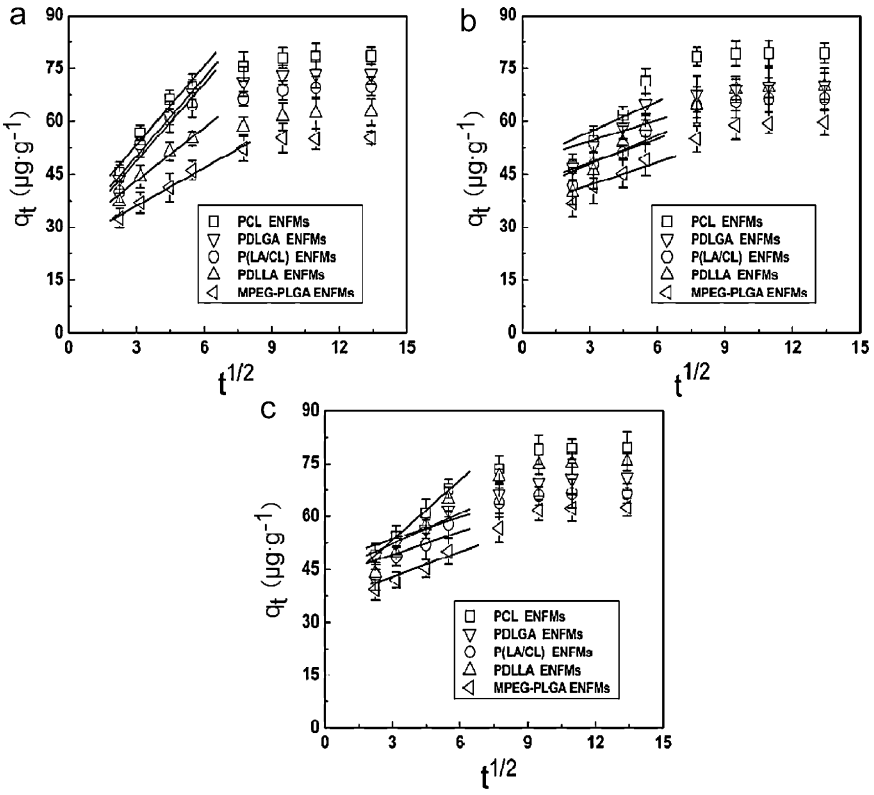

Fig. 4. Weber and Morris model for the adsorption of ANT (a), BaA (b) and BaP (c) on five ENFMs.

factor in the sorption processes of BaA and BaP on MPEG-PLGA and PDLLA ENFMs due to their larger pore sizes and volumes.

As seen from Fig. 4, the plots were not linear throughout the experiments, suggesting that more than one process affected the sorption. In our study, the sorption process of PAHs on the ENFMs sorbents involved three steps. The front linear portions demonstrated a rapid sorption stage, which included two steps: (i) the diffusion of PAH molecules from the bulk solution to the external surfaces of the ENFMs, (ii) PAH molecules adsorption onto those easily accessible hydrophobic sites on the surface (internal or external), which is often assumed to be an extremely fast step, and (iii) the later plateaus indicated the equilibrium stages after the completion of external surface coverage, where intra sorbent diffusion was dominating and the PAH molecules migrated slowly to less accessible sites in the ENFMs through a pore filling or intra diffusion process. This step is often slow due to the extremely low PAH concentration remaining in the solution. This three-stage sorption is similar to results reported in other literatures [32,34,35].

3.3. Sorption isotherms

Sorption isotherms for ANT, BaA and BaP on the five ENFMs are shown in Fig. 5. PCL and P(LA/CL) ENFMs with relatively higher surface areas (shown in Table 1) resulted in much lower equilibrium concentration in the aqueous phase, suggesting higher sorption capacity. As can be seen in Fig. 5a, the equilibrium concentration of ANT was 1.2 $\mu g\,L^{-1}$ for the PCL ENFMs system, and that was 1.8 $\mu g\,L^{-1}$ when P(LA/CL) ENFMs were used, which indicated that the sorption capacity of PCL ENFMs (surface area: 8.57 $m^2\,g^{-1}$) for ANT was larger than P(LA/CL) ENFMs (6.96 $m^2\,g^{-1}$). But the sorption capacities of PCL ENFMs for BaA and BaP were lower than those of P(LA/CL) ENFMs (see Fig. 5b and c). Since the P(LA/CL) polymer is more hydrophobic than PCL, and the water solubilities of BaA and BaP are much lower than ANT (shown in Table S1), BaA and BaP are easier to distribute on the surface of P(LA/CL) ENFMs, indicating the importance of the hydrophobicity of sorbents during PAH sorption. This can be also used to interpret that the PDLGA ENFMs with smaller surface area can sorb more ANT than PDLLA ENFMs from aqueous solution. Moreover, we noted that both the surface area and the hydrophobicity of PDLGA ENFMs were higher than those of MPEG-PLGA ENFMs, but the sorption capacity of PDLGA ENFMs for BaP was lower than that of MPEG-PLGA ENFMs, as shown in Fig. 5c. This likely due to the fact that the larger pore volume of the MPEG-PLGA ENFMs, which can provide more sorption sites for BaP molecules. Therefore, the sorption capacities of different ENFMs for PAHs are related to their morphology and properties, including surface areas, hydrophobicity and pore volume.

For a given ENFMs, a lower adsorbed mass was observed for relatively larger sorbates, and the sorption capacity of the ENFMs for the three PAHs followed the trend of ANT > BaA > BaP, this is consistent with the increasing order of their molecular volume. First, larger molecules occupy more space than relatively smaller ones on the surface of sorbents with the same attachment area. Second, larger molecules would have lower adsorption capacity in the pores of sorbents than relatively smaller ones because of the bottleneck of pores for PAH molecular diffusion [36]. In our study, the decline of sorption capacity of PDLGA ENFMs with increasing PAH molecular volume was obvious (from 178.6 to 112.3 $\mu g\,g^{-1}$). By contrast, changes in the PCL and P(LA/CL) ENFMs were both tiny, which may be ascribed to their relatively higher surface area; the lower PAH solution concentrations may have contribute to these changes as well. Furthermore, the phenomenon of the bottleneck of pores in PDLLA and MPEG-PLGA ENFMs was also not obvious due to the large pore size of these fibers, which resulted in a little decline of sorption capacity.

Isotherm fitting with model equations is critical to the exploration of sorption mechanisms. Three widely used models, including FM, PAM and PDAM, were adopted to describe our exper-

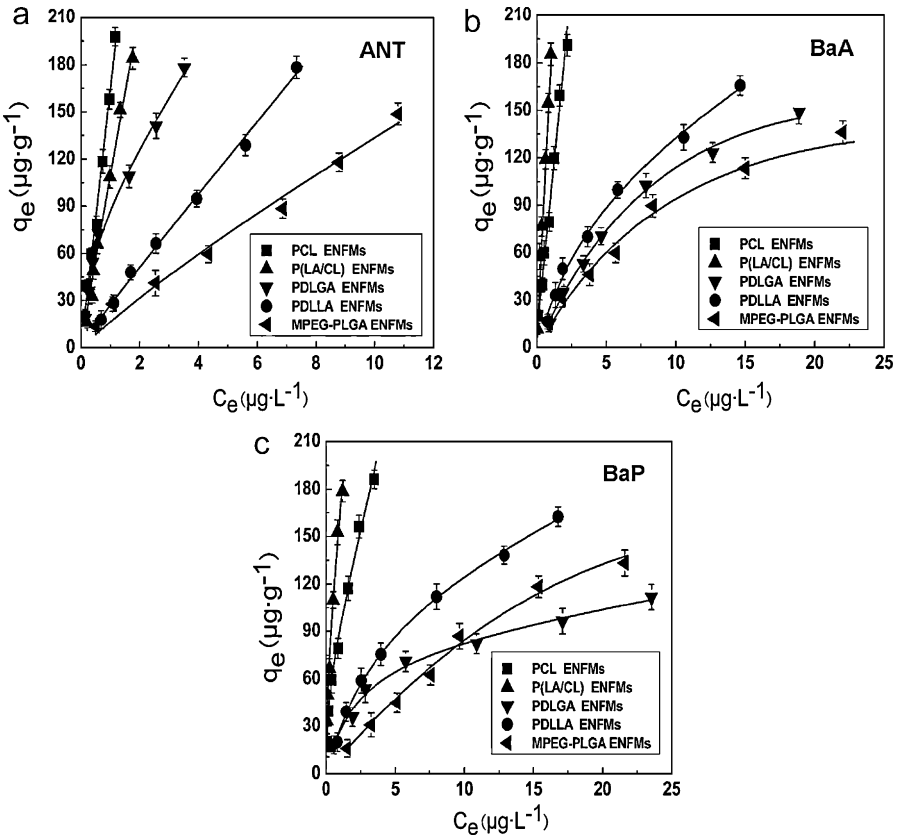

Fig. 5. Sorption isotherms of ANT (a), BaA (b) and BaP (c) on five ENFMs fitted by partition-adsorption model.

imental data. The fitted results of the PAM, FM and PDAM are shown in Fig. 5, Figs. S1 and S2, respectively. The fitted parameters for all isotherms are summarized in Table S3.

As shown in Fig. 5 and Table S3, the sorption isotherms of ANT, BaA and BaP on five ENFMs can be fitted best by the PAM, supported by the relatively higher r^2 and lower MWSE values among all tested models. The PAM used in this work was the Langmuir-type adsorption-partitioning model, which assumed "site type" for Langmuir adsorption and was a combination of the Langmuir model and the Freundlich model. Its major differences from the Freundlich model are that it reverts to linearity at very low aqueous concentration and usually has a maximum capacity for adsorption [37]. However, it was declared that the sorption data of the three PAHs on PCL, P(LA/CL) and PDLGA ENFMs in our experimental systems were difficult to accurately estimate the sorption capacities by using the PAM, since the overall sorption behaviors were dominated by partitioning in the observed concentration range, which were reflected by that the estimated partitioning contribution accounted for the bulk of the total amount of PAHs sorbed on these ENFMs [37]. Although the sorption capacities in our studies were difficult to be accurately estimated, the sorption capacities (Q^0) of PAHs on ENFMs are theoretically higher than those obtained from the PAM. More specifically, the sorption capacity of ANT on PCL ENFMs was higher than $4112.3 \pm 35.5\ \mu g\ g^{-1}$, and the sorption capacities of BaA and BaP on P(LA/CL) ENFMs were higher than 1338.8 ± 16.9 and $712.1 \pm 7.8\ \mu g\ g^{-1}$, respectively. Indeed, the estimated Q^0 values from Langmuir model were obviously higher than those obtained from the PAM (data not shown). Nevertheless, for the sorption of BaA and BaP on MPEG-PLGA ENFMs, the total sorption was dominated by the adsorption component, and the estimated sorption capacity (Q^0) of BaP was only $146.1 \pm 3.4\ \mu g\ g^{-1}$. For MPEG-PLGA ENFMs, monomethoxy polyethylene glycol (MPEG) contains –OH groups (see Fig. 1), which may cause the MPEG-PLGA ENFMs to become relatively hydrophilic than other ENFMs, and lead to the suppression of adsorption of PAHs with high hydrophobicity ($\log K_{ow}$) from aqueous solution. Consequently, the sorption capacities of different ENFMs for the three PAHs are not only related to the morphology and properties of ENFMs, including surface area, hydrophobicity and pore volume, but also influenced by the physicochemical properties of the PAHs themselves.

3.4. Sorption mechanism

The experimental results indicated that the hydrophobicity of ENFMs exhibited significant effects on their sorption rate and capacity for PAHs, further demonstrating that hydrophobic interactions played an important role in the sorption of PAHs. Moreover, the good fit of the PSOM for the kinetics data indicated that the chemical interactions were possibly involved in the sorption processes [33], which was consistent with the possible π–π bonding interactions introduced by the PAH molecules that contain π electrons interacting with the π electrons of the C=O on the polymer surface (see Fig. 1 and Fig. S3). Furthermore, for MPEG-PLGA ENFMs, the –OH groups on the their surface can act as hydrogen-bonding donors and form hydrogen bonds with organic molecules [36], which indicated that hydrogen bonding interactions played a role in the MPEG-PLGA ENFMs sorption system.

Comparing the fitted results between PAM and PDAM, we found that the sorption data of PAHs on PDLLA and MPEG-PLGA ENFMs could be also well fitted by PDAM (see Fig. S2 and Table S3), indicating that pore-filling existed in these sorption processes. This is accessible since the PDLLA and MPEG-PLGA ENFMs are more porous than other ENFMs. Considering the larger pore volume and the relatively hydrophilic property of MPEG-PLGA ENFMs, the pore-filling may be the main sorption mechanism of BaA and BaP on MPEG-PLGA ENFMs. But for the less porous PCL, P(LA/CL) and

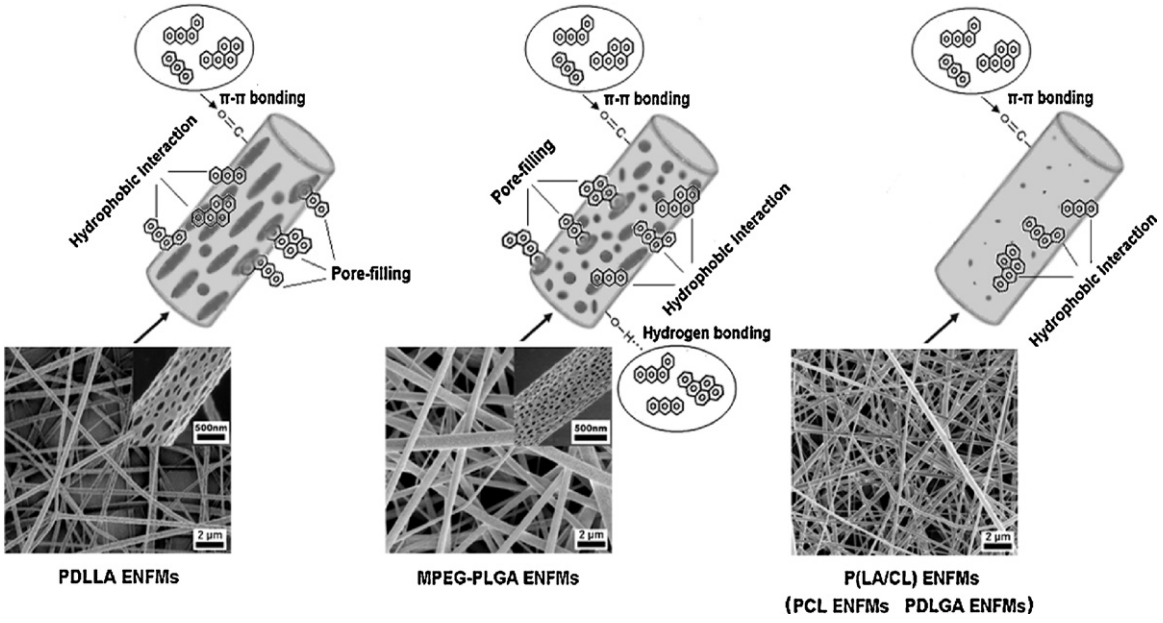

Fig. 6. Schematic diagram of the sorption of three PAHs on PDLLA ENFMs (a); MPEG-PLGA ENFMs (b); P(LA/CL), PCL and PDLGA ENFMs (c).

PDLGA ENFMs, the pore-filling mechanism was negligible, and the hydrophobic interaction became the main mechanism for sorption, thus the partitioning dominated the sorption processes of three PAHs on PCL, P(LA/CL) and PDLGA ENFMs.

Therefore, it can be concluded that the sorption mechanisms of the five ENFMs for PAHs were different (shown in Fig. 6). The hydrophobic interactions and pore-filling were the main mechanisms for the sorption of three PAHs on PDLLA ENFMs, while the hydrophobic interactions dominated the PAH sorption on PCL, P(LA/CL) and PDLGA ENFMs. The sorption mechanisms of MPEG-PLGA ENFMs were relatively complicated, which mainly included pore-filling, hydrogen bonding interactions and hydrophobic interactions. Furthermore, π–π bonding interactions may be also involved in the PAH sorption of all the ENFMs.

4. Conclusions

Five types of ENFMs were used as sorbents for removing PAHs from aqueous solution. The sorption kinetics results showed high sorption rates and achievement of sorption equilibrium after 3 h. The PSOM can describe the sorption kinetics of the three PAHs on the five ENFMs well, and the sorption isotherm data in this study were fitted best by the PAM. The fitting results showed that the sorption kinetics and sorption capacity of different ENFMs were related to their surface area, hydrophobicity and pore volume. The sorption mechanisms of three PAHs on the five ENFMs showed some differences. The hydrophobic interactions, hydrogen bonding interactions, π–π bonding interaction and pore-filling were found to exist in the PAH sorption on ENFMs.

In our study, PCL and P(LA/CL) ENFMs were found to be favorable sorbents for PAHs in terms of their sorption kinetics and sorption capacity. The sorption capacity of ANT on PCL ENFMs was higher than $4112.3 \pm 35.5\ \mu g\ g^{-1}$, and the sorption capacities of BaA and BaP on P(LA/CL) ENFMs were higher than 1338.8 ± 16.9 and $712.1 \pm 7.8\ \mu g\ g^{-1}$, respectively. Since the morphology and structure of ENFMs can be adjusted by altering the electrospinning parameters, it is possible to further optimize ENFMs to increase their sorption capacities. Furthermore, the polymers are optional for different pollutants. The abovementioned properties, combined with their advantage of operational simplicity, indicate that ENFMs may become potential sorbents for PAH removal from wastewater and drinking water if designed properly.

Acknowledgements

This work was supported by the National Basic Research Program of China (973 Program, 2010CB429003), the Key Project of Chinese Ministry of Education (No. 109026), and Program for Changjiang Scholars and Innovative Research Team in University (No. IRT0809) of China.

Appendix A. Supplementary data

Supplementary data associated with this article can be found, in the online version, at doi:10.1016/j.jhazmat.2011.06.055.

References

[1] Z. Wang, J.W. Chen, P. Yang, F.L. Tian, X.L. Qiao, H.T. Bian, L.K. Ge, Distribution of PAHs in pine (Pinus thunbergii) needles and soils correlates with their gas-particle partitioning, Environ. Sci. Technol. 43 (2009) 1336–1341.
[2] X.L. Wan, J.W. Chen, F.L. Tian, W.J. Sun, F.L. Yang, K. Saiki, Source apportionment of PAHs in atmospheric particulates of Dalian: factor analysis with nonnegative constraints and emission inventory analysis, Atmos. Environ. 40 (2006) 6666–6675.
[3] L.L. Wang, Z.F. Yang, J.F. Niu, J.Y. Wang, Characterization, ecological risk assessment and source diagnostics of polycyclic aromatic hydrocarbons in water column of the Yellow River Delta, one of the most plenty biodiversity zones in the world, J. Hazard. Mater. 169 (2009) 460–465.
[4] L. Bezalel, Y. Hadar, P.P. Fu, J.P. Freeman, C.E. Cerniglia, Initial oxidation products in the metabolism of pyrene, anthracene, fluorene, and dibenzothiophene by the white rot fungus *Pleurotus ostreatus*, Appl. Environ. Microbiol. 62 (1996) 2554–2559.
[5] J.E. Jung, D.S. Lee, S.J. Kim, D.W. Kim, S.K. Kim, J.G. Kim, Proximity of field distribution of polycyclic aromatic hydrocarbons to chemical equilibria among air, water, soil, and sediment and its implications to the coherence criteria of environmental quality objectives, Environ. Sci. Technol. 44 (2010) 8056–8061.
[6] H.S. Wang, Z. Cheng, P. Liang, D.D. Shao, Y.A. Kang, S.C. Wu, C. Wong, M.H. Wong, Characterization of PAHs in surface sediments of aquaculture farms around the Pearl River Delta, Ecotoxicol. Environ. Saf. 73 (2010) 900–906.
[7] A. Malik, P. Verma, A.K. Singh, K.P. Singh, Distribution of polycyclic aromatic hydrocarbons in water and bed sediments of the Gomti River, India, Environ. Monit. Assess. 172 (2011) 529–545.
[8] J.Y. Cho, J.G. Son, B.J. Park, B.Y. Chung, Distribution and pollution sources of polycyclic aromatic hydrocarbons (PAHs) in reclaimed tidelands and tidelands of the western sea coast of South Korea, Environ. Monit. Assess. 149 (2009) 385–393.

[9] J.H. Sun, G.L. Wang, Y. Chai, G. Zhang, J. Li, J.L. Feng, Distribution of polycyclic aromatic hydrocarbons (PAHs) in Henan reach of the Yellow River, middle China, Ecotoxicol. Environ. Saf. 72 (2009) 1614–1624.
[10] S.N. Chu, S. Sands, M.R. Tomasik, P.S. Lee, V.F. McNeill, Ozone oxidation of surface-adsorbed polycyclic aromatic hydrocarbons: role of PAH–surface interaction, J. Am. Chem. Soc. 132 (2010) 15968–15975.
[11] O.T. Woo, W.K. Chung, K.H. Wong, A.T. Chow, P.K. Wong, Photocatalytic oxidation of polycyclic aromatic hydrocarbons: intermediates identification and toxicity testing, J. Hazard. Mater. 168 (2009) 1192–1199.
[12] J. Sabate, J.M. Bayona, A.M. Solanas, Photolysis of PAHs in aqueous phase by UV irradiation, Chemosphere 44 (2001) 119–124.
[13] J.F. Niu, P. Sun, K.W. Schramm, Photolysis of polycyclic aromatic hydrocarbons associated with fly ash particles under simulated sunlight irradiation, J. Photochem. Photobiol. A 186 (2007) 93–98.
[14] A.K. Haritash, C.P. Kaushik, Biodegradation aspects of polycyclic aromatic hydrocarbons (PAHs): a review, J. Hazard. Mater. 169 (2009) 1–15.
[15] R.J. Krupadam, M.S. Khan, S.R. Wate, Removal of probable human carcinogenic polycyclic aromatic hydrocarbons from contaminated water using molecularly imprinted polymer, Water Res. 44 (2010) 681–688.
[16] S. Changchaivong, S. Khaodhiar, Adsorption of naphthalene and phenanthrene on dodecylpyridinium-modified bentonite, Appl. Clay Sci. 43 (2009) 317–321.
[17] Z.Q. Gong, K. Alef, B.M. Wilke, P.J. Li, Activated carbon adsorption of PAHs from vegetable oil used in soil remediation, J. Hazard. Mater. 143 (2007) 372–378.
[18] C. Long, J.D. Lu, A.M. Li, D.B. Hu, F.Q. Liu, Q.X. Zhang, Adsorption of naphthalene onto the carbon adsorbent from waste ion exchange resin: equilibrium and kinetic characteristics, J. Hazard. Mater. 150 (2008) 656–661.
[19] K. Yang, L.Z. Zhu, B.S. Xing, Adsorption of polycyclic aromatic hydrocarbons by carbon nanomaterials, Environ. Sci. Technol. 40 (2006) 1855–1861.
[20] A. Greiner, J.H. Wendorff, Electrospinning: a fascinating method for the preparation of ultrathin fibers, Angew. Chem. Int. Ed. 46 (2007) 5670–5703.
[21] D. Li, Y.N. Xia, Electrospinning of nanofibers: reinventing the wheel? Adv. Mater. 16 (2004) 1151–1170.
[22] N. Bhardwaj, S.C. Kundu, Electrospinning: a fascinating fiber fabrication technique, Biotechnol. Adv. 28 (2010) 325–347.
[23] Z.G. Wang, L.S. Wan, Z.M. Liu, X.J. Huang, Z.K. Xu, Enzyme immobilization on electrospun polymer nanofibers: an overview, J. Mol. Catal. B: Enzym. 56 (2009) 189–195.
[24] S. Agarwal, J.H. Wendorff, A. Greiner, Use of electrospinning technique for biomedical applications, Polymer 49 (2008) 5603–5621.
[25] T.J. Sill, H.A. von Recum, Electrospinning: applications in drug delivery and tissue engineering, Biomaterials 29 (2008) 1989–2006.
[26] V. Thavasi, G. Singh, S. Ramakrishna, Electrospun nanofibers in energy and environmental applications, Energy Environ. Sci. 1 (2008) 205–221.
[27] N. Kattamuri, J.H. Shin, B. Kang, C.G. Lee, J.K. Lee, C. Sung, Development and surface characterization of positively charged filters, J. Mater. Sci. 40 (2005) 4531–4539.
[28] Q. Xu, S.Y. Wu, M. Wang, X.Y. Yin, Z.Y. Wen, W.N. Ge, Z.Z. Gu, Electrospun nylon6 nanofibrous membrane as SPE adsorbent for the enrichment and determination of three estrogens in environmental water samples, Chromatographia 71 (2010) 487–492.
[29] D.J. Qi, X.J. Kang, L.Q. Chen, Y.Y. Zhang, H.M. Wei, Z.Z. Gu, Electrospun polymer nanofibers as a solid-phase extraction sorbent for the determination of trace pollutants in environmental water, Anal. Bioanal. Chem. 390 (2008) 929–938.
[30] B. Pan, B.S. Xing, Adsorption kinetics of 17 alpha-ethinyl estradiol and bisphenol A on carbon nanomaterials. I. Several concerns regarding pseudo-first order and pseudo-second order models, J. Soils Sediments 10 (2010) 838–844.
[31] B. Pan, K. Sun, B.S. Xing, Adsorption kinetics of 17 alpha-ethinyl estradiol and bisphenol A on carbon nanomaterials. II. Concentration-dependence, J. Soils Sediments 10 (2010) 845–854.
[32] Q. Yu, R.Q. Zhang, S.B. Deng, J. Huang, G. Yu, Sorption of perfluorooctane sulfonate and perfluorooctanoate on activated carbons and resin: kinetic and isotherm study, Water Res. 43 (2009) 1150–1158.
[33] Z.H. Cheng, X.S. Liu, M. Han, W. Ma, Adsorption kinetic character of copper ions onto a modified chitosan transparent thin membrane from aqueous solution, J. Hazard. Mater. 182 (2010) 408–415.
[34] W.H. Cheung, Y.S. Szeto, G. McKay, Intraparticle diffusion processes during acid dye adsorption onto chitosan, Bioresour. Technol. 98 (2007) 2897–2904.
[35] M.J. Yuan, S.T. Tong, S.Q. Zhao, C.Q. Jia, Adsorption of polycyclic aromatic hydrocarbons from water using petroleum coke-derived porous carbon, J. Hazard. Mater. 181 (2010) 1115–1120.
[36] K. Yang, B.S. Xing, Adsorption of organic compounds by carbon nanomaterials in aqueous phase: Polanyi theory and its application, Chem. Rev. 110 (2010) 5989–6008.
[37] G.S. Xia, W.P. Ball, Adsorption-partitioning uptake of nine low-polarity organic chemicals on a natural sorbent, Environ. Sci. Technol. 33 (1999) 262–269.